

## Observation of Hybrid Soliton Vortex-Ring Structures in Bose-Einstein Condensates

Naomi S. Ginsberg,<sup>1</sup> Joachim Brand,<sup>2</sup> and Lene Vestergaard Hau<sup>1</sup><sup>1</sup> Department of Physics and Division of Engineering and Applied Sciences, Harvard University, Cambridge, Massachusetts 02138<sup>2</sup> Max Planck Institute for the Physics of Complex Systems, 01187 Dresden, Germany  
(Dated: April 14, 2024)

We present the experimental discovery of compound structures comprising solitons and vortex rings in Bose-Einstein condensates (BECs). We examine both their creation via soliton-vortex collisions and their subsequent development, which is largely governed by the dynamics of interacting vortex rings. A theoretical model in three-dimensional (3D) cylindrical symmetry is also presented.

PACS numbers: 03.75.Lm, 47.37.+q, 47.32.Cc, 42.50.Gy

Quantized vortices have long been considered a signature of superfluidity in Helium II [1]. The recent emergence of Bose-condensed alkali gases provides a new and different arena for studying quantum fluids, their excitations, and interactions of the latter. In addition to observing vortices alone [2, 3, 4], experimentalists have reported observations of grey solitons [5, 6] and their decay into vortex rings (VR) [7, 8] via the Kadomtsev-Petviashvili, or "snake", instability [9].

In this Letter, we present the observation of a new class of topological excitations in BECs: hybrid structures originating from a combination of solitons and VRs. By "soliton", we mean a non-dispersive nonlinear wave whose phase profile and velocity are determined by its amplitude. Solitonic wavefronts extend on 2D sheets whereas vortex structures have a depleted core and phase singularity along a 1D filament, which may loop to form a VR. We detail how these nonlinear excitations initially collide and how the subsequent compound structure dynamics diverge from those of the superposed evolution of individual excitations. To date, the interplay between solitons and vortices has only been explored theoretically [10, 11, 12].

In previous work [8], we studied grey solitons and vortices generated from the quantum analog of shock waves by creating a single, narrow density defect in a BEC. We presently optimize the likelihood of collisions between these excitations by creating two symmetrically placed defects via a mechanism similar to that used in [8].

A thin wire blocks the "coupling" beam from illuminating the center of a magnetically trapped BEC (Fig. 1 (a)), to create a symmetric double light-roadblock. We then inject two counter-propagating Gaussian-shaped "probe" pulses along the symmetry axis of the trap. The pulses compress spatially by several orders of magnitude via the slow-light technique [14], and ultimately "entirely" inside the BEC. The probe beams are resonant with the atom  $s'$  internal  $|j_i\rangle\text{--}|j_i\rangle$  transition while the coupling beam is resonant with the  $|j_i\rangle\text{--}|j_i\rangle$  transition (Fig. 1 (b)).

When the pulses arrive at the wire's shadow, their propagation is effectively arrested and they are further compressed, as their speed depends on the coupling beam

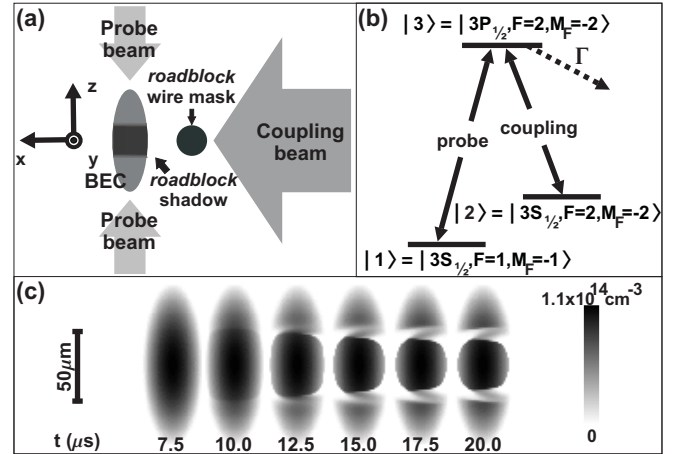


FIG. 1: D defect creation. (a) Double light-roadblock setup. (b) Energy level diagram;  $M_F$  refers to the projection of the atom  $s'$  angular momentum along the magnetic field quantization axis,  $z$ , of the 4-D ee electromagnetic trap [13]. (c) D density plots of 4D ee sodium atoms from 2D simulations of defect creation using a 60  $\mu\text{m}$  wire mask; initially, the BEC has  $4.0 \times 10^6$  atoms. Light pulse intensities and durations are as in the experiment.

intensity that rapidly falls to zero at the borders of this region [8]. Subsequently, atoms at the halted pulses' locations are ejected, having first been transferred from initial state,  $|j_i\rangle$ , to  $|j_i\rangle$  (untrapped) via a slow-light induced dark state. This results in two deep, narrow density defects in  $|j_i\rangle$ , symmetric about the BEC's center (Fig. 1 (c)).

For the current experiment, we condense  $3.6 \times 10^6$  sodium atoms in  $|j_i\rangle$  and employ magnetic trap frequencies  $\omega_z = 2 \times 21 \text{ Hz}$  and  $\omega_x = \omega_y = 3.0 \times \omega_z$ . We work at temperatures well below the transition temperature to BEC so there is virtually no non-condensed component. The coupling (peak probe) Rabi frequency is  $2 \times 15.3 \text{ (3.8) MHz}$ , and duration (probe 1/e half-width) is  $12 \text{ (2.5) } \mu\text{s}$ . We use a 35  $\mu\text{m}$  wire mask.

After creating the defects, we vary the duration of condensate evolution in the magnetic trap,  $t_{\text{trap}}$ , and then release the condensate and let it expand for  $t_{\text{exp}} = 19.9$

ms before using a slice technique [8, 15] to image the central 20–30  $\mu\text{m}$  thick slab of the expanded cloud in the  $x$ - $z$  plane. Figure 2(a) shows the ‘control’ experiment in which a single probe pulse is injected into the BEC, while Fig. 2(b) depicts the double-roadblock experiment in which interactions between excitations are evident. In both cases, the data are highly reproducible.

The early dynamics that ensue from the creation of a single defect are detailed in Fig. 3 of [8]. The defect splits into two density dips propagating at the sound speed in the  $+z$  and  $-z$  directions, while the back edge of each steepens due to the density dependence of the sound speed. In a classical fluid, this would lead to shock wave formation i.e. the back edges would develop infinite slope. In a superfluid, significant density changes over distances shorter than the healing length cannot occur [16].

Consequently, as the density dips travel, they shed grey solitons each time their back edges become too steep [8]. As observed in Fig. 2(a), the solitons, although stable in 1D, kink and decay into vortex structures via the snake instability, seeded predominantly by the transverse density variation of the condensate depicted in Fig. 1(c).

We now describe the experimental data in Fig. 2, comparing and contrasting the double-defect images with the control experiment, before considering a corresponding theoretical simulation. Focusing mostly on structures between the two initial defects, we see at  $t_{\text{trap}} = 0.1$  ms in Fig. 2(b) that solitons (pale stripes) have already shed from density dips originally emanating from the defects. High-density bands on the top and bottom result from the rush of fluid into the defect locations. The first solitons shed are the deepest, hence slowest moving, and therefore bound the regions of high density. In the center, between these first solitons, secondly shed ones have kinked so that they overlap on the sides but not in the middle, forming a checkerboard pattern. This is clearly seen at  $t_{\text{trap}} = 0.4$  ms where the images also show VR cores in the ‘four corners’. Figure 2(b) at 0.1 and 0.4 ms and Fig. 2(a) at 0.5 ms are comparable. The single-defect image shows additional shallower solitons in the wake of the travelling density dip, that are initially hidden in the double-defect version by the mirror image of higher-contrast structures. At  $t_{\text{trap}} = 1.1$  ms (Fig. 2(b)), soliton curvature has increased even more. Like at 1.3 ms of Fig. 2(a), the deepest solitons form double-cusped shapes (W’ on the top, M’ on the bottom) that span the cloud from side to side. The second pair of solitons propagate toward one another further, closing off a region of fluid in the center.

We have explored the 3D structure of the excitations by varying the  $y$ -position of the imaged slice to find that the system is highly cylindrically symmetric. Thus, the white loop in the center at 1.1 ms and the pairs of attenuated lobes seen in the shots corresponding to  $t_{\text{trap}} = 1.3$  and 1.7 ms represent roughly ellipsoidal shells of low density, a feature clearly absent in the single-defect case.

Comparing the latter two time-points with  $t_{\text{trap}} = 2.1$  ms in Fig. 2(a), we conclude that the centers of the deepest solitons have decayed into VRs, forming the equatorial components of their corresponding closed low density shells in Fig. 2(b). The upper and lower hemispheres of the shells all derive from solitons formed after the first (deepest) ones that produced VRs.

At  $t_{\text{trap}} = 2.3$  ms in Fig. 2(b), the closed structures appear to interlace and subsequently form a single low density shell at the center of the condensate (2.8–6.0 ms). This provides very strong evidence that the double-defect dynamics are not merely a superposition of mirrored single-defect dynamics. At  $t_{\text{trap}} = 4.1$  ms, Fig. 2(a) displays a soliton fragment in the center with a VR below. At 4.4 ms in Fig. 2(b), the low density structure is closed and could not be formed from the superposition of elements from the corresponding time point in Fig. 2(a). Despite being larger at  $t_{\text{trap}} = 5$  and 6 ms (Fig. 2(b)) than in previous frames, this compound structure is temporarily stable. At 6.6 ms, we observe that what was a closed shell has sheared and come apart at the sides. The resulting structures break cylindrical symmetry, highlighting their sensitivity to torque from the laser beams, evident in Fig. 1(c). Furthering the case for interactions rather than superposition, the last two frames of Fig. 2(a) have a long-lived VR in the center, in stark contrast with Fig. 2(b) at 6.6 ms, which has segments that could not be constructed from VRs alone.

We measure the soliton and shell halfwidths to range from 3 to 6  $\mu\text{m}$ , comparable to a calculated healing length of 4  $\mu\text{m}$  [17]. We also note the collective modes in the BEC produced by the initial rush of fluid into the defects’ locations. The high density bands in both Figs. 2(a) and 2(b) bend, contract, and expand. We find these modes are highly dependent on the initial defect shape.

To complement our observations, we have performed simulations based upon a generalized Gross-Pitaevskii (GP) description [18] for three phases of BEC evolution as follows: We first simulate defect creation via slow-light propagation on a 2D spatial grid, as in Fig. 1(c). The atoms in  $|\psi_i\rangle$  are quickly ejected from the trap and we map a symmetrized version of the resulting defect in the  $|\psi_i\rangle$  condensate onto a 3D cylindrically symmetric grid [19]. We then calculate in-trap evolution of the  $|\psi_i\rangle$  atoms for a duration  $t_{\text{trap}}$  and finally continue to follow the BEC evolution after the trapping potential is turned off.

The results of simulations for  $t_{\text{exp}} = 14$  ms with varying  $t_{\text{trap}}$  are shown in Fig. 3. (After 14 ms of cloud expansion, all topological dynamics are frozen out and further evolution simply leads to spatial magnification of the developed features; the BEC’s aspect ratio differs from that at 19.9 ms by  $\sim 15\%$ .) We see the same prominent features in the simulation as in the experiment, allowing us to identify the nature of the low density shells. Phase information confirms the existence of solitons and identifies the creation and annihilation of VRs. As we

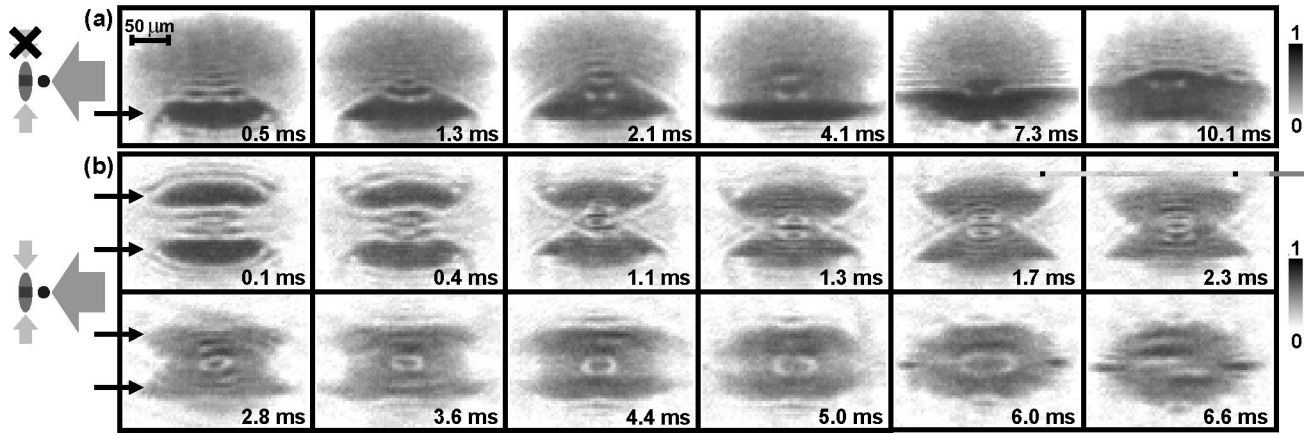


FIG. 2: Experimentally observed resonant transmission in ages of BECs (transmitted laser intensity normalized to incident) after they are illuminated with coupling and probe pulse(s). In (a) ((b)), one (two) probe pulse(s) is (are) hitting the cloud, there are initially  $4.0$  ( $3.6$ )  $10^6$  condensed atoms, and the imaged slice is  $30$  ( $23$ )  $\mu\text{m}$  thick. Times cited refer to evolution time in trap,  $t_{\text{trap}}$ , after defect creation;  $t_{\text{exp}} = 19.9$  ms. A row(s) indicate initial defect plane(s).

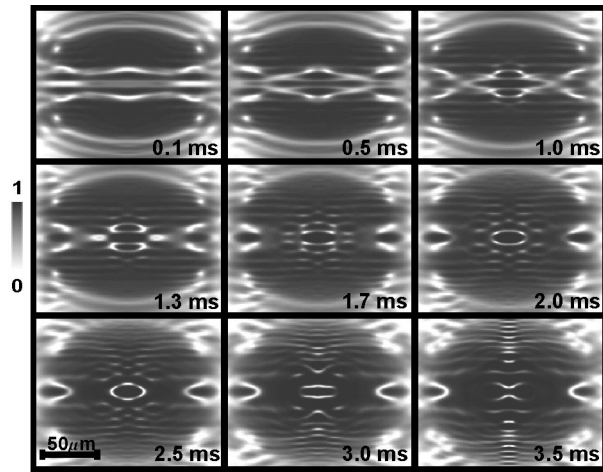


FIG. 3: Simulation for  $t_{\text{exp}} = 14$  ms ( $t_{\text{trap}}$  on plots) with parameters the same as in Fig. 1 (c). To compare with experiment, we plot  $e^{D_y(x;z)}$ , where  $D_y(x;z)$  is the optical density along  $y$  over the central  $22$   $\mu\text{m}$  slab of the BEC.

detail below, the simulations indicate that the expansion ‘re-stabilizes’ solitons that would have been subjected to the snake instability, if kept in the trap. Experimental parameters have been chosen to cover a regime in which VRs are produced but parent solitons are not destroyed.

The simulation follows that of the experiment up to  $t_{\text{trap}} = 1.3$  ms, after which point evolution is slightly accelerated. Other discrepancies include reduced soliton curvature and less dramatic collective mode breathing than in the experiment. This could be a result of the different initial defect separation used in the theory to generate a sequence most comparable to the data. The simulation’s cylindrical symmetry is an added approximation, but it generally describes the observations well.

Despite these differences, the simulations provide us

with the history of the experimentally observed structures that must be expanded to be optically resolved. Calculations show that if two solitons are incident on one another, the time that it takes them to reach each other and their degree of kinking at that point have different density dependencies. During expansion but before interaction energy is completely converted to kinetic, soliton translational velocity and the rate of soliton kinking both decrease as BEC density drops, but at different rates. These different density dependencies do not only imply that expansion evolution is highly important and different than in-trap evolution [20]; they also lead to the notion that expansion sequences succeeding two different in-trap durations are not mere duplicates of set from each other in time. We see variations in such sequences, typically manifested by the occurrence of VR creation and annihilation at slightly different points in the evolution.

As an example, we present the simulated release dynamics for  $t_{\text{trap}} = 3.0$  ms in Fig. 4. As in the experiment, the first soliton (blue) shed from each of the waves traveling toward the BEC’s center is the deepest, slowest, and least stable, leading to decay into VRs at  $t_{\text{exp}} = 1.5$  ms. Solitons created after the first ones (green through red, in order of creation from top defect) propagate across the center line of the BEC ( $t_{\text{exp}} = 1.5$  and  $3.0$  ms); those with opposite propagation directions sometimes overlap. As the third and fourth generated solitons reach the newly formed VRs on the side opposite whence they originated, we observe pairs of low density shells ( $t_{\text{exp}} = 4.0$  ms). By examining the phase, we confirm, as discussed for images 1.3 and 1.7 ms of Fig. 2 (b), that these shells are made from VRs and transiently passing soliton fronts.

The second deepest (secondly shed, green) solitons cross in the center of the BEC as their midpoints bend toward one another (also  $t_{\text{exp}} = 4.0$  ms). As these fronts reach the VRs at 5.0 ms (again forming a pair of low

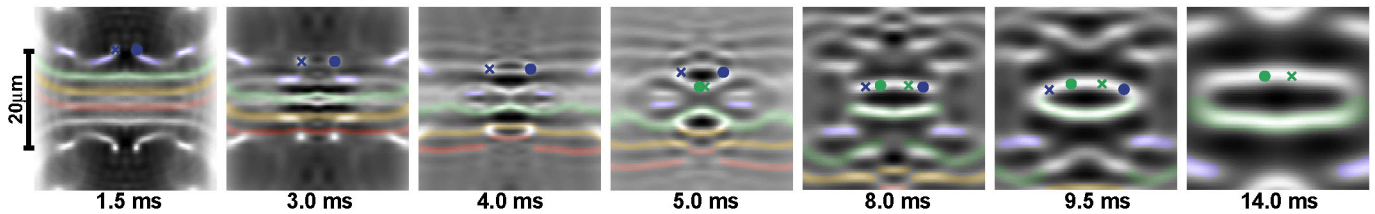


FIG. 4: Simulation of soliton VR dynamics during expansion after  $t_{\text{trap}} = 3.0$  m s. Times cited are  $t_{\text{exp}}$ . Only solitons propagating in  $z$  direction (downward) from the  $+z$  (top) defect are shaded (blue through red, in order of creation), to assist in tracking them over time of each frame to frame. Dots (crosses) indicate vortex cores for  $z > 0$  only with positive (negative) circulation with respect to the plane of the page. The vortex colors correspond to parent soliton colors, although the green cores are generated by the mirror image of the correspondingly shaded soliton. Density ranges from 0 to  $7.5, 4.5, 4.1, 3.6, 1.3, 0.92, 0.42 \text{ g cm}^{-3}$  for each of the times presented, respectively. Simulation parameters are the same as in Fig. 1 (c).

density shells), the central portions of the solitons curve further, producing within themselves two smaller VRs with opposite circulation from the larger ones. These truly hybrid low density structures, consisting of parent soliton segments and VRs, 'dislocate' from the rest of the soliton fronts. They each comprise two concentric VRs embedded in a roughly hemispherical solitonic shell. The smaller VRs are evident from the wavefunction's phase even though they are not distinguishable in the density plots. The general motion of the hybrid segments is largely determined by the velocity fields from the vortices present. Like an umbrella turning inside-out, the curvature of these hybrid structures reverses through  $t_{\text{exp}} = 8.0$  m s, as the inner rings propel themselves away from one another and the outer rings propel toward the center line. This occurs in the experiment for  $t_{\text{trap}} = 2.3$  m s and in Fig. 3 at 1.7 m s. The VRs behave as the 'phantom' propellers in the compound structures.

As the outer VRs propagate toward each other, a closed shell forms from the two hybrid segments ( $t_{\text{exp}} = 9.5$  m s). It is an ellipsoidal solitonic shell incorporating four VRs of alternating circulation that encircle the structure like lines of constant latitude on a globe. The outer VRs eventually annihilate (quantized circulation at the VR cores disappears). Subsequently, the two segments that formed the central shell lose their curvature, and the shell breaks up along  $z = 0$ . This is seen at  $t_{\text{exp}} = 14$  m s (a close-up of the BEC at  $t_{\text{trap}} = 3.0$  m s in Fig. 3) and should be compared to the experimentally observed shearing at 6.6 m s in Fig. 2 (b).

In light of these observations it is natural to ask whether low density shells can exist as stationary states in a BEC. We have shown that the GP equation exhibits stationary solutions in spherical symmetry consisting of an inner sphere of almost constant density surrounded by low density shells close to Bessel-function type spherical standing waves  $\sin(kr) = r$  known from the linear Schrödinger equation. This has been independently treated by others [21]. The infinite space solutions have an infinite number of particles and concentric shells. In a trap, similar solutions with finite particle

number and number of shells are possible; details will be given elsewhere. Unlike the observed structures discussed above, the spherical stationary states show no vortex core structures. However, the observed hybrid shells might play a role in the decay of the stationary solutions.

In brief, we have presented the experimental observation and theoretical confirmation of low density shells in a fully 3D BEC, consisting of complex hybrid soliton vortex-ring structures. VR propulsion, attraction, and annihilation heavily influence the structures' dynamics. The BEC's decreasing density, after a conning trap is switched on, contributes critically to the dynamics, as the resulting regime is on the cusp of stability of solitons typically subject to the snake instability in 3D.

The authors thank Z. Dutton and S. Komineas for fruitful discussion and insights. This work was supported by AFOSR, NSF, NASA, and the ARO-MURIP program.

---

Electronic address: ginsber@fas.harvard.edu

- [1] R. J. Donnelly, *Quantized Vortices in Helium II* (Cambridge Univ. Press, Cambridge, UK, 1991).
- [2] M. R. Matthews et al., *Phys. Rev. Lett.* 83, 2498 (1999).
- [3] K. W. Madison, F. Chevy, W. Wohlleben, and J. Dalibard, *Phys. Rev. Lett.* 84, 806 (2000).
- [4] J. R. Abo-Shaeer, C. Raman, J. M. Vogels, and W. Ketterle, *Science* 292, 476 (2001).
- [5] S. Burger et al., *Phys. Rev. Lett.* 83, 5198 (1999).
- [6] J. Denschlag et al., *Science* 287, 97 (2000).
- [7] B. P. Anderson et al., *Phys. Rev. Lett.* 86, 2926 (2001).
- [8] Z. Dutton, M. Budde, C. Slowe, and L. V. Hau, *Science* 293, 663 (2001).
- [9] B. B. Kadomtsev and V. I. Petviashvili, *Sov. Phys. Dokl.* 15, 539 (1970); C. A. Jones, S. J. Putterman, P. H. Roberts, *J. Phys. A* 19, 2991 (1986); C. Josserand and Y. Pomeau, *Europhys. Lett.* 30, 43 (1995); D. L. Feder et al., *Phys. Rev. A* 62, 053606 (2000); A. M. Uryshv et al., *Phys. Rev. Lett.* 89, 110401 (2002).
- [10] J. Brand and W. P. Reinhardt, *J. Phys. B* 34, L113 (2001); J. Brand and W. P. Reinhardt, *Phys. Rev. A* 65, 043612 (2002).
- [11] S. Komineas and N. Papanicolaou, *Phys. Rev. A* 68,

- 043617 (2003).
- [12] N. G. Berloff, *Phys. Rev. A* **69**, 053601 (2004).
- [13] L. V. Hau et al., *Phys. Rev. A* **58**, R54 (1998).
- [14] L. V. Hau, S. E. Harris, Z. Dutton, and C. H. Behroozi, *Nature* **397**, 594 (1999).
- [15] M. Andrews et al., *Science* **275**, 637 (1997).
- [16] C. J. Pethick and H. Smith, *Bose-Einstein Condensation in Dilute Gases* (Cambridge Univ. Press, UK, 2002).
- [17] Y. Castin and R. Dum, *Phys. Rev. Lett.* **77**, 5315 (1996).
- [18] Z. Dutton and L. V. Hau, *Phys. Rev. A* in press, quant-ph/0404018.
- [19] Density in the 2D simulation was normalized and then interpolated. The result was averaged with its mirror image about  $z$  and then scaled by the 3D BEC ground state density for the same number of atoms.
- [20] It is not as critical to distinguish between in-trap and expansion evolution in the single-defect case since its geometry does not lead to the possibility of soliton collisions.
- [21] M. Machholm and H. Smith, private communication; L. D. Carr and C. W. Clark, cond-mat/0408460.